Dielectric modelling of optical spectra of thin In_2O_3 : Sn films

2002 J. Phys. D: Appl. Phys. 35 794

(http://iopscience.iop.org/0022-3727/35/8/311)

INSTITUTE OF PHYSICS PUBLISHING JOURNAL OF PHYSICS D: APPLIED PHYSICS
J. Phys. D: Appl. Phys. **35** (2002) 794–801 PII: S0022-3727(02)31723-6

Dielectric modelling of optical spectra of thin In_2O_3 : Sn films

D Mergel[1] **and Z Qiao**

Physics Department, WG Thin Film Technology, University Essen, 45117 Essen, Germany

E-mail: Dieter.Mergel@Uni-Essen.De

Received 10 December 2001
Published 2 April 2002
Online at stacks.iop.org/JPhysD/35/794

Abstract
Optical transmittance spectra of In_2O_3 : Sn (ITO) films were simulated with a computer program based on dielectric modelling. The films were prepared by radiofrequency sputtering under various oxygen fluxes such that the carrier density varies from 3×10^{19} to 1.5×10^{21} cm^{-3}. The dielectric function used is the sum of three types of electronic excitations: intraband transitions of free electrons (Drude model), band gap transitions, and interband transitions into the upper half of the conduction band. The parameters of these excitations are evaluated as a function of the carrier density. The damping in the Drude term was modelled frequency-dependent to account for the low extinction coefficient observed in the visible spectral range. The parameters resulting from the optical measurements were compared with those from the electrical measurements. Both the optical mobility and carrier density are found to be higher than those of the respective electric parameters. These discrepancies are attributed to a pronounced microstructure with badly conducting grain boundaries. The refractive index at 550 nm decreases linearly with increasing electron concentration. This is due both to the shift of the plasma edge and the Burstein–Moss shift of the band edge. All band gap transitions go up to the Fermi level.

1. Introduction

Thin films of In_2O_3 : Sn (ITO) are widely used as transparent electrodes. The electrical properties of the n-type semiconductor ITO are controlled over several orders of magnitude by Sn donors and their deactivation by interstitial oxygen [1, 2]. In state-of-the-art sputter procedures, resistivities ρ down to 150 $\mu\Omega$ cm are achieved [3]. The electrical properties are determined by density N_{dc} and direct current mobility μ_{dc} of the free electrons in the conduction band. The fundamental relation for the electrical conductivity $\sigma = 1/\rho$ of a homogeneous medium is

$$\sigma = N_{dc} e \mu_{dc} \tag{1}$$

The maximum value of μ_{dc} reported so far is about 100 cm^2 V^{-1} s^{-1} obtained in flux-grown single crystals [4] or modulation-doped evaporated films [5], whereas in sputtered films maximally 70 cm^2 V^{-1} s^{-1} has been achieved [6]. An intrinsic limit for the correlation of N_{dc} and ρ was established theoretically for the case that scattering at ionized donors is the dominant friction process for electron motion [7]. The relationship can be reformulated for N_{dc} and μ_{dc} by means of equation (1).

The optical properties of ITO films were studied in detail by reflectance and transmittance spectrometry [8] and by ellipsometry [9]. The transmittance window is limited towards higher wavelengths by the plasma edge due to free carrier transitions and towards lower wavelengths by the band edge. There is a smooth onset of absorption at the band edge which was explained by an Urbach tail [8] or by indirect transitions [9, 10], in addition to a direct band gap.

Within the framework of the Drude theory, the density of free electrons determines the position of the plasma edge. The mobility is related to the damping of the electron oscillations, which in turn determines the width of the plasma edge. Only few authors checked this relationship experimentally.

In this work, optical transmittance spectra are fitted with a computer model based on dielectric modelling [11]. Several

[1] Author to whom correspondence should be addressed.

models for the band gap and the free electron transitions are tried. The fit parameters of film thickness, electron density and mobility are compared with the corresponding values obtained from mechanical profilometry and electrical measurements, respectively. The films were prepared by radiofrequency sputtering at various oxygen fluxes such that the carrier density varies from 3×10^{19} to $1.5 \times 10^{21}\,\mathrm{cm}^{-3}$. The deposition process and its influence on structural and electrical properties are described elsewhere [6].

2. Experimental and computational methods

2.1. Sample preparation and characterization

The films were prepared by radiofrequency diode sputtering of an oxidic target. The substrate temperature was 380°C. The Ar flux was 20 sccm with an O_2 admixture of 0–10%. The glass substrates (Schott, BK7) measured 26 mm × 26 mm. The density and the direct current mobility of the free electrons were determined by the Hall effect and conductivity measurements in van der Pauw geometry [12]. The carrier density N_{dc} varies from 3×10^{19} to $1.5 \times 10^{21}\,\mathrm{cm}^{-3}$.

Transmittance spectra in the range 180 nm to 3 μm were measured in a Perkin-Elmer Lambda-19 spectrometer. A spectrum for a sample with $N_{\mathrm{dc}} = 4.25 \times 10^{20}\,\mathrm{cm}^{-3}$ is shown in figure 1 together with simulated spectra.

2.2. Spectra simulation by dielectric modelling

The theoretical exposition in this and the following section is based on [8, 9, 13]. The laboratory forms of the formulae used to evaluate the spectra numerically are summarized in table 1.

The susceptibility χ of an isotropic medium is defined by

$$P = \varepsilon_0 \chi E \tag{2}$$

where P is the polarization of the medium and E is the external electric field. χ is taken as the sum of individual susceptibilities

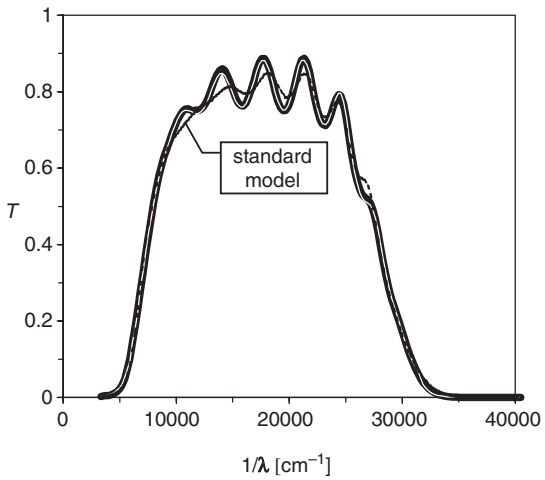

Figure 1. Experimental transmittance spectrum and its simulation with the standard (- - - -) and the modified dielectric model. The curve for the modified model is shown as a white line inside the recorded spectrum, because the calculated curve matches the experimental one.

χ_i arising from various physical mechanisms of polarization. The complex dielectric function ε relative to vacuum is given as

$$\varepsilon = \varepsilon_{\mathrm{re}} + i\varepsilon_{\mathrm{im}} = 1 + \sum_i \chi_i \tag{3}$$

The complex refractive index $\tilde{n}$ is the square root of ε:

$$\tilde{n} = n + \mathrm{i}k = \sqrt{\varepsilon_{\mathrm{re}} + \mathrm{i}\varepsilon_{\mathrm{im}}} \tag{4}$$

where n is the refractive index and k is the extinction coefficient. Reflectance and transmittance spectra of thin films, $R(\lambda)$ and $T(\lambda)$, respectively, can be calculated when the optical functions $n(\lambda)$ and $k(\lambda)$ in the spectral region of interest and the film thickness d are known.

Dielectric modelling of optical spectra comprises several steps. (1) Formulae for the χ_i with free parameters are set up. (2) Initial values of the free parameters and of d are assumed. (3) Optical spectra are calculated and compared with their experimental counterparts. The parameters of χ_i and d are then varied so that the simulated spectra approach the experimental ones. We use the commercial computer program SCOUT 98 [11] which applies a downhill simplex method to find the optimal fit parameters.

2.3. Dielectric model for ITO

The optical properties of ITO in the spectral range of interest, 200 nm to 3 μm, are controlled by three types of electronic excitations: band gap transitions, interband transitions from the bulk of the valence band into the bulk of the conduction band, and intraband transitions of the electrons in the conduction band. They are, in a first approximation, modelled with standard formulae available in the fit program. The variables and parameters used in these and other formulae referred to later are listed in table 1.

The classical Drude formula is used for the susceptibility of free electrons:

$$\chi_{\mathrm{Dr}}(\omega) = -\left[\frac{\Omega_{\mathrm{Dr}}^2}{\omega^2 + \Gamma_{\mathrm{Dr}}^2}\right] + \mathrm{i}\left(\frac{\Gamma_{\mathrm{Dr}}}{\omega}\right)\left[\frac{\Omega_{\mathrm{Dr}}^2}{\omega^2 + \Gamma_{\mathrm{Dr}}^2}\right] \tag{5}$$

with ω being the frequency, defined with the physical units s^{-1}, eV or cm^{-1}. Γ_{Dr} is a damping constant. The Drude frequency Ω_{Dr} is given as

$$\Omega_{\mathrm{Dr}}^2 = \frac{e^2 N_{\mathrm{Dr}}}{\varepsilon_0 m_{\mathrm{eff}}} \tag{6}$$

Table 1. Nomenclature.

Variable or Parameter	Description	Equation no.
	Angular frequencies [s^{-1}, eV or cm^{-1}]	
ω		
Ω_{Dr}	Drude frequency	(5), (6)
Ω_{P}	Plasma frequency, $\varepsilon_{\mathrm{re}}(\Omega_{\mathrm{P}}) := 0$	(7)
Γ_{Dr}	Damping of Drude oscillations	(5)
	Densities [cm^{-3}]	
N_{Dr}	Carrier density from Ω_{Dr}	(6)
N_{dc}	Direct current carrier density from Hall effect	(1)
	Mobilities [$cm^2\,V^{-1}\,s^{-1}$]	
M_{Dr}	Mobility of Drude oscillations, derived from Γ_{Dr}	(10)
μ_{dc}	Direct current mobility	(1)

Here, N_{Dr} is the free electron density, m_{eff} is the effective mass at the bottom of the conduction band, e is the elementary charge and ε_0 is the vacuum permittivity. The response of the free carriers to an optical excitation corresponds to a high pass filter.

Equation (6) can be used to obtain the free carrier density from optical spectra when the effective mass is known. We designate the electron density thus obtained by N_{Dr}, whereas the carrier density derived from direct current Hall effect measurements is called N_{dc}. The effective mass m_{eff} can be determined when the Drude frequency and the carrier density are known from optical and Hall effect measurements, respectively, provided that the density of optically active carriers is the same as that of the electrically active carriers.

The longitudinal plasma frequency Ω_P is obtained by setting $\varepsilon_{re} = 0$, yielding

$$\Omega_P = \sqrt{\frac{\Omega_{Dr}^2}{\varepsilon_\infty} - \Gamma_{Dr}^2} \tag{7}$$

where ε_∞ is the value of the dielectric function in the relevant spectral region around Ω_P arising from all transitions except the Drude oscillations. Sometimes, Ω_{Dr} is also called plasma frequency. However, this may cause confusion; hence, we prefer the name 'Drude frequency'. The strong increase of absorption and reflection in the spectrum at the plasma frequency Ω_P is called plasma edge.

For the band gap transitions, we first use the model of O'Leary–Johnson–Lim (OJL) [14] that has been proposed to model the band gap of amorphous silicon. It is based on parabolic densities of states below and above the mobility gap E_g and on exponential tails that are characterized by damping constants, γ_v and γ_c, for the valence and conduction bands, respectively. The imaginary part of χ is derived from the joint density of states. The real part is then obtained by a Kramers–Kronig transformation of the imaginary part. This procedure is implemented in the SCOUT 98 program.

The interband transitions into the upper half of the conduction band are represented by a harmonic oscillator. This is a simplification because the UV dielectric spectrum of semiconductors usually exhibits a variety of critical points and lines. Nevertheless, the model is sufficient because only the low-energy tail of the corresponding susceptibility is relevant for the transitions in the spectral range below 40 000 cm^{-1} (5 eV).

The frequency-dependent susceptibilities resulting from a fit of the three aforementioned transitions to the spectrum of figure 1 are shown in figure 2, designated by 'stand'. The region where T is detectably larger than zero is indicated by vertical dashed lines. The imaginary part, indicated by the shaded area, looks like a band pass limited to lower energies by the free carrier excitations and to higher energies by the interband transitions. The real part, ε_{re} ('stand., re'), satisfies the Kramers–Kronig relation (KKR) and exhibits a negative and a positive divergence when the frequency approaches 0 or Ω_{HO} (here 45 800 cm^{-1}), respectively. The contribution of the free electrons to ε_{re} is shown in the lower part of figure 2. It is always negative.

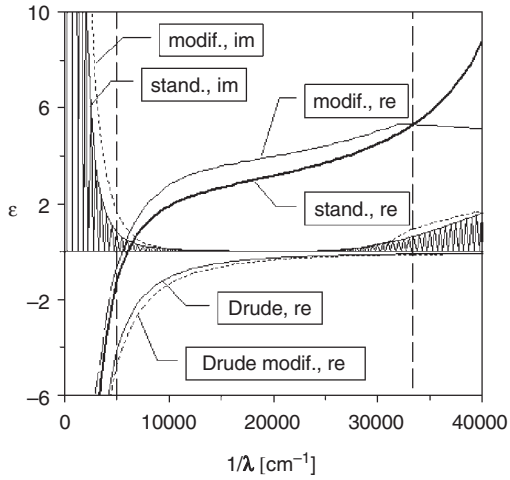

Figure 2. Dielectric function (real and imaginary part) used to simulate the spectra of figure 1. Calculated with the standard and the modified model.

3. Results and direct conclusions

3.1. Standard model

A spectral fit with the standard model is shown by the dotted line in figure 1. The average experimental spectrum is well represented but its specific features are reproduced badly. The fit misses the positions and amplitudes of the interference extrema and also the correct curvature of the plasma edge. The deviations arise because the optimal fit of the Drude model predicts a very strong absorption in the visible region. If, in a suboptimal fit, the parameters are tuned to yield a better fit in the visible, the curvature at the plasma edge becomes too steep. There are also some deviations in the band gap region indicating that the OJL model cannot account for the smooth onset of absorption at the band edge.

We have refined the Drude model and applied a different band gap model that allows for direct and indirect transitions. This yields a visually satisfying fit to the experimental spectrum (see the white line within the experimental curve in figure 1), with a standard deviation of 0.003 instead of 0.017 before. The details of the refined models are discussed in the following sections.

3.2. Refined Drude model with frequency-dependent damping

In order to get a better fit to the curvature of the plasma edge, a frequency-dependent damping factor with four fit parameters is introduced:

$$\Gamma_{Dr}(\omega) = \Gamma_L - \frac{(\Gamma_L - \Gamma_H)}{\pi}\left[\arctan\left(\frac{\omega - \Omega_{\Gamma Dr}}{\Gamma_{\Gamma w}}\right) + \frac{\pi}{2}\right] \tag{8}$$

Γ_L and Γ_H represent the low-frequency ($\omega = 0$) and high-frequency ($\omega =$ infinite) damping factor, respectively. The changeover frequency and the width of the function are designated by $\Omega_{\Gamma Dr}$ and $\Gamma_{\Gamma Dr}$, respectively. A frequency-dependent damping term in a Drude description has been explained in terms of ionized impurity scattering [8].

The resulting optimal $\Gamma_{Dr}(1/\lambda)$ curves are shown in figure 3 for four samples. The Drude frequencies are indicated by vertical bars. The changeover frequency $\Omega_{\Gamma Dr}$

is proportional to the plasma frequency, $\Omega_{\Gamma Dr} \sim 0.75\Omega_{Dr}$, also for the samples not represented in figure 3. For the samples with $\Omega_{Dr} > 8000\,cm^{-1}$, the low-frequency damping factor scatters around $1800\,cm^{-1}$ (0.22 eV), whereas the high-frequency damping factor is at least one order of magnitude lower and sometimes nearly reduced to zero on this scale. This is consistent with the literature. Values of 0.2 eV ($1600\,cm^{-1}$) below and 0.05 eV ($400\,cm^{-1}$) above Ω_{Dr} are reported for a film with an electron density of 1.3×10^{21} cm^{-3} ($\Omega_{Dr} =$ 1.4 eV, $11\,300\,cm^{-1}$) [8]. The corresponding values for [15] are 0.24 eV ($1900\,cm^{-1}$) and 0.1 eV ($800\,cm^{-1}$) as can be evaluated from the detailed data given in that reference.

Equation (8) is successful because more fitting parameters are introduced. As an alternative, we modelled the plasma edge using the standard Drude formula plus a harmonic oscillator [16]. This approach, too, yields a good fit to the experimental curves with an oscillator frequency of about 0.6 of the Drude frequency. In order to check the reliability of the various models we have compared the optically determined thickness with that obtained from profilometry and obtain $d_{opt}/d_{stylus} =$ 1.00(10) and 0.95(3) for the standard and the $\Gamma_{Dr}(\omega)$ models, respectively. The number in parentheses is the standard deviation (of the sample set) of the last digit(s). The lowest standard deviation, namely 2%, is obtained for the Drude plus oscillator model: $d_{opt}/d_{stylus} = 0.98(2)$. Ratios smaller than 1 are physically meaningful because profilometry measures the top height whereas the optical interferences average over the roughness of the film surface. We have no third method to determine the thickness of the films and use the standard deviation of the ratio to check the quality of the fit models.

The success of the modified models proves that the fit of the classical Drude formula yields a very strong absorption for frequencies above the Drude frequency.

The mobility of the free carriers is derived from the damping constant via the average collision time $\langle\tau\rangle$:

$$\langle\tau\rangle = \frac{1}{\Gamma_{Dr}} \tag{9}$$

$$M_{Dr} = \frac{e\langle\tau\rangle}{m_{eff}} \tag{10}$$

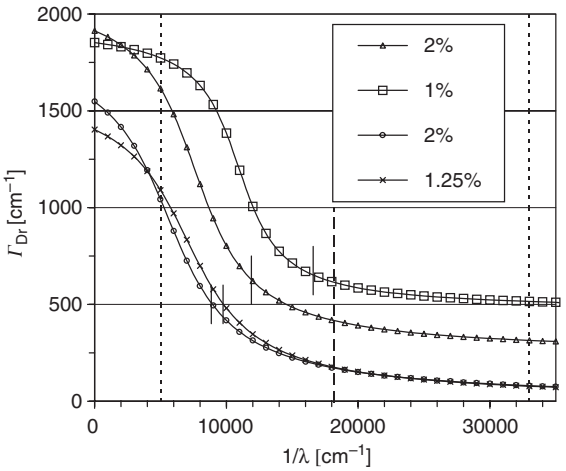

Figure 3. Frequency-dependent damping factor $\Gamma_{Dr}(1/\lambda)$ for four representative samples.

The mobility thus obtained is designated by M_{Dr} whereas μ_{dc} is used for the mobility obtained from equation (1) by means of the direct current Hall effect and conductivity measurements. The damping constant is found to be about 100–1000 cm^{-1} in the measured spectral region corresponding to collision times of 53–5.3 fs and to mobilities of about 267–26.7 $cm^2\,V^{-1}s^{-1}$.

In figure 4, the mobilities derived from the original and the refined Drude models are compared with the electrically determined values of μ_{dc}. It is evident that the optical mobility is independent of the direct current mobility. The mobility M_{Dr} at $0\,cm^{-1}$ is approximately constant and generally lower than μ_{dc}. The mobilities at the Drude frequency are generally higher than μ_{dc}. They reach values of about $100\,cm^2\,V^{-1}\,s^{-1}$ corresponding to the maximum value reported for single crystals [4].

Equation (6) predicts the square of the Drude frequency to be proportional to the free electron density. Therefore, in figure 5, Ω_{Dr}^2 from the various models is plotted versus N_{dc}

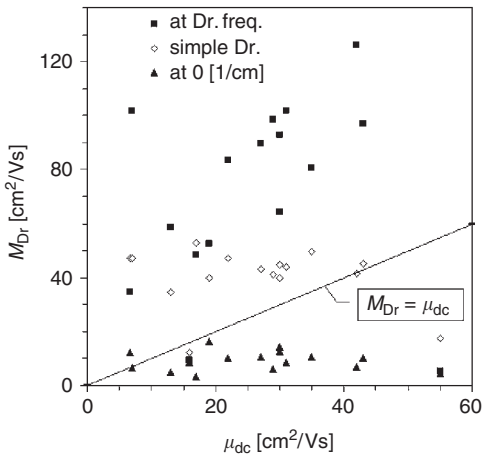

Figure 4. Optically determined mobilities M_{Dr} versus direct current mobility μ_{dc}. For the frequency-dependent damping, the values at the Drude frequency Ω_{Dr} and at $1/\lambda = 0\,cm^{-1}$ are displayed.

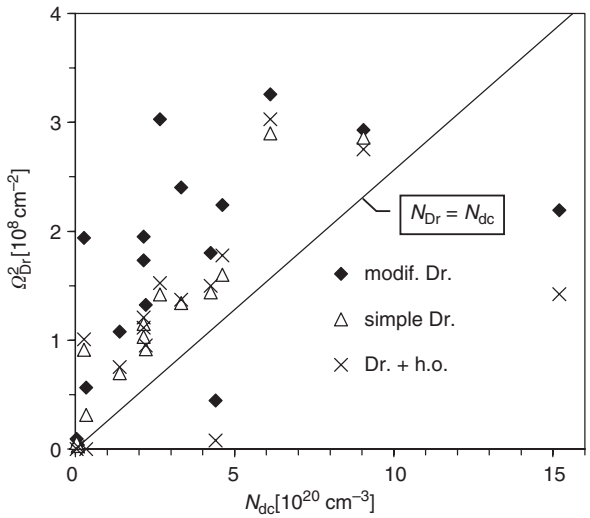

Figure 5. Square of the Drude frequency, Ω_{Dr}^2, for various models of the plasma edge as a function of the electrically determined electron density N_{dc}. The diagonal line represents Ω_{Dr}^2 calculated from N_{dc} with an effective electron mass of $0.35m_e$.

obtained from the Hall effect. The diagonal represents the values of Ω_{Dr}^2 for an effective electron mass of $0.35m_e$, the value reported in [15]. The free electron density, derived directly from Ω_{Dr}^2 by means of equation (6), is called N_{Dr}. The diagonal in figure 5 represents the case $N_{Dr} = N_{dc}$. The great majority of data points lie above this diagonal. For these points, a direct evaluation of the free electron density by means of equation (6) yields values (N_{Dr}) larger than N_{dc}. This means that there are optically active carriers that do not contribute to the direct current. Their fraction is about 0.5.

Results similar to those represented in figure 5 have been found in an investigation on ZnO [17]: the square of the Drude frequency is a linear function of N_{dc} with a non-zero ordinate intercept.

3.3. Band gap with direct and indirect transitions

For direct transitions, we try a square-root dependence of the joint density of states above the direct band gap E_{d0}:

$$\Phi_{dir}(\omega) = D\sqrt{(\hbar\omega - E_{d0})}[1 - \text{step}(E_{d1})] \qquad (11)$$

The step function limits the square-root dependence to energies below E_{d1}. Indirect transitions are modelled according to

$$\Phi_{ind}(\omega) = I(\hbar\omega - E_{ind})^2 \qquad (12)$$

The interband transitions into the upper half of the conduction band are represented by a harmonic oscillator above E_{d1}.

Heavily doped ITO is a degenerate semiconductor. The Fermi level lies inside the conduction band so that band gap transitions are shifted towards higher energies with increasing conduction electron density. This effect, known as the Burstein–Moss (BM) shift, is described by

$$\Delta E_g^{BM} = \left(\frac{\hbar^2}{2m_{vc}^*}\right)(3\pi^2 n_e)^{2/3} \qquad (13)$$

where n_e is the density of electrons in the conduction band and m_{vc}^* is the combined effective mass of the conduction and the valence band, defined by

$$\frac{1}{m_{cv}^*} = \frac{1}{m_c^{eff}} + \frac{1}{m_v^{eff}} \qquad (14)$$

The BM shift is discussed in detail in [8, 9]. It has to be taken into account when band gap transitions are modelled.

When the transitions lead to the minimum in the conduction band that experiences the BM shift, the formulae have to be multiplied by a step function that suppresses transitions into states below the Fermi level. Depending on the assumed band model, only the direct or the indirect or both transitions experience the BM shift. For the direct transitions, the energy of transitions to the Fermi level was termed E_{Fd}. We have tried several models, but obtained basically the same result: all characteristic energies increase with increasing carrier density, not only those related to E_{Fd}.

The parameters E_{OJL}, E_{ind}, E_{d0} and E_{Fd} are displayed in figure 6 as a function of $N_{Dr}^{2/3}$. All follow the same trend. From fitting a straight line to $E_{Fd}(N_{Dr}^{2/3})$, we obtain, via equation (13), a combined effective mass $m_{vc}^{eff} = 0.58$. This compares with values 0.54 [15] and 0.525 [8] in the literature. Using equation (16), the three values yield valence band effective masses $m_{vc}^{eff}/m_e = -0.9, -1, -1$. The negative sign arises from the fact that $m_{vc}^{eff} > m_c^{eff}$ and would imply that the valence band is curved in the same direction as the conduction band [15]. The situation is, however, more complicated because a band gap narrowing occurs due to scattering. If this effect is taken into account, positive values $m_v^{eff}/m_e = 0.6$–1 are obtained [8].

In the literature, band gaps of $E_{ind} = 2.40$–3.65 eV ($19\,000$–$29\,500$ cm^{-1}) and $E_{dir} = 3.5$–3.85 eV ($28\,000$–$31\,000$ cm^{-1}) for zero electron density are reported; for an overview see [9]. Our values for $N_{Dr} = 0$ are close to the lower limits of the reported ranges.

3.4. Contributions to ε and n at 550 nm

Figure 7 shows the contributions of the considered three electronic excitations to ε at $\lambda = 550$ nm as a function of

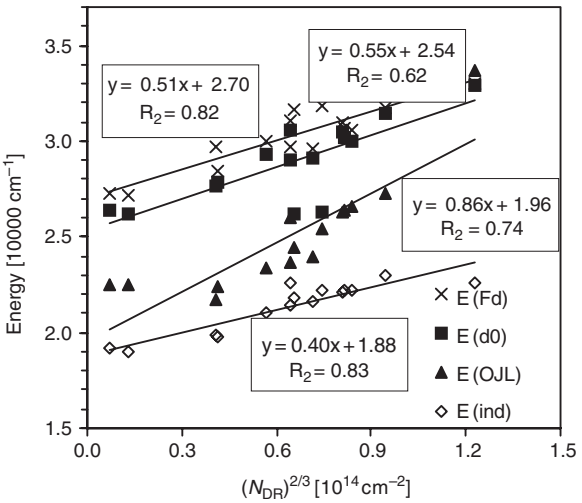

Figure 6. Band gap energies as a function of $N_{Dr}^{2/3}$, with N_{Dr} being the optically determined carrier density. E(Fd): Fermi level; E(d0): direct band gap; E(ind): indirect band gap; E(OJL): band gap of the OJL model.

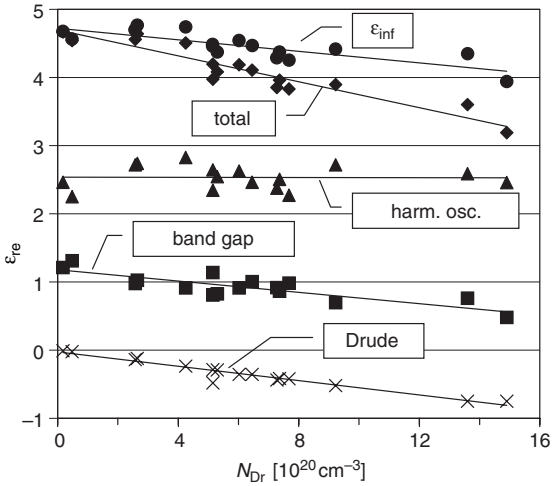

Figure 7. Value of the dielectric function at 550 nm and its contributions from free carriers (Drude term), ε_{Dr}, band gap transitions, ε_{BG}, and bulk interband transitions, ε_{HO}, modelled by a harmonic oscillator. ε_{inf} designates all contributions except the Drude term.

the carrier density N_{Dr}. The relationships are approximately linear. The Drude term is always negative. This is to be expected because the plasma wavelength is always larger than 550 nm and approaches this value with increasing N_{Dr}. This leads to an increasing value of ε_{re} due to the KKR. The maximum size is $\varepsilon_{Dr} = 0.84$ for $N_{Dr} = 1.5 \times 10^{21}\,cm^{-3}$. The band edge term due to direct and indirect transitions decreases with increasing N_{Dr}. This is explained by the BM shift of the transitions to higher energies, away from 550 nm, and its influence on ε_{re} via the KKR. The contribution of the harmonic oscillator, representing transitions into the upper half of the conduction band, is nearly independent of N_{Dr}, as is to be expected.

The total dielectric function changes from 4.6 for $N_{Dr} = 0$ to 3.1 for $N_{Dr} = 1.5 \times 10^{21}\,cm^{-3}$. This decrease is equally due to a stronger free carrier absorption and the shift of the band edge. The contribution of the interband transitions plus vacuum ($\varepsilon = 1$) is 4.45 ± 0.2. This is referred to as ε_{inf} in the literature where values between 3.7 and 4.6 are reported; see e.g. [9] for a review. A dependency of ε_{inf} on the free electron concentration has not been explicitly stated up to now. However, data that show such a relationship have sometimes been reported. For radiofrequency sputtered films, it was found that ε_{inf} decreases from 4 for an electron density of $0.2 \times 10^{20}\,cm^{-3}$ to 3 for $5 \times 10^{20}\,cm^{-3}$ [18]. Our results are very close to those of [9] where $\varepsilon_{inf} = 4.48 \pm 0.15$ was obtained by ellipsometry with the tendency to decrease with increasing N_{Dr}. For our data, we obtain

$$\varepsilon_{inf} = 4.7 - 0.4 \times 10^{-21}\,[cm^3] N_{Dr} \qquad (15)$$

When applying the OJL model instead of the direct and indirect transitions, the band gap contribution to ε (550 nm) is nearly zero. However, the variation of the harmonic oscillator term becomes larger so that within $\pm 1\%$ the same values as above are obtained for ε_{inf}.

The refractive index n decreases with the free electron density according to

$$n = 2.17 - 0.24 \times 10^{-21}[cm^3] N_{Dr} \qquad (16)$$

n is reduced from 2.17 to 1.81 for the maximum carrier density $N_{Dr} = 1.5 \times 10^{21}\,cm^{-3}$. For radiofrequency magnetron sputtered films, a variation of the refractive index between 1.83 and 2.15 is reported with n being smaller for annealed films [19]. The maximum carrier concentration was 1.5×10^{21}. This is in agreement with equation (16).

4. Discussion

4.1. Electronic properties

The carrier densities N_{Dr} and N_{dc}, determined optically from the Drude frequency Ω_{Dr} and electrically by the Hall effect, respectively, are linearly correlated; see figure 5. N_{Dr} is larger than N_{dc} in the majority of cases. This may be explained by isolated regions of the film that do not contribute to the direct current. The films consist of a mixture of grains with different orientations, similar to the microstructure reported in [6]. Grain sizes, determined from XRD spectra, range from 15 to 50 nm, except for (100)-oriented grains where values up to 200 nm are observed. Such a microstructure was explained by oxygen incorporation into the lattice at the surface of the growing film and segregation of oxygen and Sn to grain boundaries in the subsurface region [20]. Our films contain about 10 at% Sn. In films with more than 5 at% Sn, an intergranular amorphous phase was revealed by transmission electron microscopy [21]. This may lead to badly conducting grain boundaries and electrically isolated grains. The surplus of Sn (10%) in our samples drives the segregation. Adding oxygen to the sputter gas and incorporating it into the film enhances this process.

The optically determined mobility M_{Dr} is independent of, and in most cases higher than, the direct current mobility μ_{dc}. This may be due to an inhomogeneous microstructure with phases of different mobility, e.g. crystalline and amorphous regions as discussed above. For direct current measurements, the current passes through the whole sample. The film acts like a network of conductors in series. The reciprocal mobilities $1/\mu_{dc}$ have to be averaged and the lower mobility determines the average μ_{dc}. The optically excited electrons move only a short distance and do not leave the grains or the grain boundaries. They oscillate in parallel and the mobilities M_{Dr} have to be averaged. As the grains occupy a much larger volume than the boundaries, M_{Dr} represents the mobility within the grains.

The mobilities at the Drude frequency reach a maximum of about $100\,cm^2\,V^{-1}\,s^{-1}$. This is the maximum value of the mobility found in flux-grown single crystals [4] or in zone-confined thin films [5]. The upper limit for degenerate ITO is determined by scattering at ionized donors [7]. Generally, the mobilities reported in the literature range from 10 to $70\,cm^2\,V^{-1}\,s^{-1}$, similar to the variation of our μ_{dc} values. Therefore, microstructural inhomogeneities of the discussed type are a general hindrance to obtain optimal resistivities.

4.2. Band gap

In the literature, several models were used to model the band gap transitions in In_2O_3 or in ITO. All of them incorporate direct allowed transitions. The minimum of the conduction band was assumed to be at $k = 0$ [8] or at $k > 0$ [22]. In order to account for the gradual onset of absorption, an Urbach tail [8] or indirect forbidden transitions [10] were assumed. In [9], indirect transitions gave a better fit to ellipsometry and reflectance data than an Urbach tail.

We have tried several models but cannot decide clearly for a specific variant. All characteristic band gap energies shift to higher values with increasing electron densities indicating that all transitions experience the BM shift. This implies that all band gap transitions go to the same conduction band minimum where the electrons are located. This result fits well to a recent band structure calculation [23]. There, the conduction band is found to be electron-like with a minimum at the Γ point. The valence band consists of many narrow and overlapping subbands. No indirect band gap is found. In terms of this model, the details of the band gap transitions should be related to details of the valence band structure.

4.3. The microstructure of the films

In all simulations reported so far, we have treated the films as homogeneous medium. It is, however, well known that thin

films are porous and that their properties may vary along the growth direction.

It is well known that the properties of thin films are not always homogeneous throughout the film. In order to take a possible gradient of the optical properties along the film normal into account, a two-layer model was tried. This approach yielded a better fit to the experimental spectra than the one-layer standard model. However, one of the layers came out to be very thin (3 nm) and exhibited properties extremely different from the thicker (about 600 nm), more ITO-like, film. A ratio $d_{\mathrm{opt}}/d_{\mathrm{stylus}} = 1.10(10)$ was found. As we had no possibility to check such a structure independently, we dropped this hypothesis. A many-layer structure is a more realistic approach. As it implies more fit parameters, it would certainly give a better fit to the spectra. This model can only be checked reasonably if additional independent information, e.g. on a concentration or density gradient, is available.

The variation of the carrier density in our films was effected by varying the oxygen pressure during deposition. This will, however, also influence the density of the films. In a work on evaporated TiO_2 films, the dependence of the refractive index on the density of the films was investigated [24]. An effective-medium approach could successfully reconcile the experimental data with the Clausius–Mosotti theory [25]. In future work, we shall incorporate such a model also in the simulation of thin film spectra. The formulae describing the data reported in figures 6 and 7 are related to effective optical parameters averaged over the whole film.

5. Conclusions

Transmittance spectra of thin ITO films were simulated with simple dielectric models. The films were regarded as a homogeneous continuous medium and the fit parameters obtained are to be regarded as effective optical constants.

The experimental plasma edge cannot be represented by the classical Drude formula. A frequency-dependent damping has to be introduced allowing for a relatively lower damping constant above the Drude frequency. This can be obtained directly by a frequency-dependent damping factor in the Drude formula or by an additional harmonic oscillator at about 0.75 of the Drude frequency. With these alterations and a band gap model with several parameters, the simulated spectra fit the experimental ones with an average error of about 0.3%.

The ratio of the optically determined thickness and that obtained by profilometry is 0.95(3) and 0.98(2) for the extended Drude formula and for the added harmonic oscillator, respectively. For the standard models, the ratio was 1.00(10). For a two-layer model, it was 1.10(10). Values below 1 are possible because the stylus glides over the peaks of the surface whereas the optical method averages over the local film thickness. The standard deviation is an indicator of the quality of the fit.

The mobility deduced from the damping constant in the range of the Drude frequency reaches $100\,\mathrm{cm^2\,V^{-1}\,s^{-1}}$. This is about the same value as that observed in single crystals where scattering at ionized donors is expected to be the dominant friction mechanism. The direct current mobility is generally much lower. The electron density deduced from the evaluation of the plasma edge is generally higher than that obtained from the Hall effect.

The discrepancies between the electrically and optically determined free electron parameters are attributed to a pronounced microstructure with badly conducting grain boundaries. Our films contain a relatively high Sn content for which the occurrence of an intergranular amorphous phase is to be expected.

The transmittance in the band gap region is successfully fitted by models comprising several parameters. All characteristic energies of these models experience a shift to larger values with increasing free electron concentration. This implies that all transitions go to the absolute minimum of the conduction band. This interpretation corresponds to recent band structure calculations which indicate that there is no indirect band gap.

The imaginary part of the dielectric function represents a band pass. As a consequence of the KKR, the real part of the dielectric function, $\varepsilon_{\mathrm{re}}$, displays a negative divergence in the region of the plasma edge and a peak in the region of the band edge. $\varepsilon_{\mathrm{re}}$ and the refractive index n in the visible spectral range decrease linearly with increasing free electron density because both edges shift to higher energies.

References

[1] Frank G and Köstlin H 1982 *Appl. Phys.* **A27** 197–206
[2] Löbl H P, Huppertz M and Mergel D 1996 *Surf. Coat. Techn.* **82** 90–8
[3] Joshi R N, Singh V P and McClure J C 1995 *Thin Solid Films* **257** 32–5
[4] Wen S J, Couturier G, Chaminade J P, Marquestaut E, Claverie J and Hagenmuller P 1992 *J. Sol. State Chem.* **101** 203–10
[5] Rauf I A 1993 *Mater. Lett.* **18** 123–7
[6] Mergel D, Schenkel M, Ghebre M and Sulkowski M 2001 *Thin Solid Films* **392** 91–7
[7] Bellingham J R, Phillips W A and Adkins C J 1992 *J. Mater. Sci. Lett.* **11** 263–5
[8] Hamberg I and Granqvist C G 1986 *J. Appl. Phys.* **60** R123–R159
[9] Weijtens C H L and van Loon P A C 1991 *Thin Solid Films* **196** 1–10
[10] Sczyrbowski J, Dietrich A and Hoffmann H 1983 *Phys. Status Solidi* a **78** 243–52
[11] Theiss M *Hard and Software for Optical Spectroscopy* Dr Bernhard-Klein-Str. 110, 52078 Aachen, Germany, www.mtheiss.com
[12] van der Pauw L J 1992 Phil. Res. Rep. **13** 1–9; see also www.eeel.nist.gov/812/hall.html
[13] Stenzel O 1996 *Das Dünnschichtspektrum. Ein Zugang von den Grundlagen zur Spezialliteratur* (Berlin: Akademie-Verlag) (in German)
[14] O'Leary S K, Johnson S R and Lim P K 1997 *J. Appl. Phys.* **82** 3334–40
[15] Köstlin H, Jost R and Lems W 1975 *Phys. Status Solidi* a **29** 87–93
[16] Monterrat E, Boy P and Marcel C 1998 *Communication at the 1998 Optical Interference Coatings Conf.*
[17] Brehme S, Fenske F, Fuhs W, Nebauer E, Poschenrieder M, Selle B and Sieber I 1999 *Thin Solid Films* **342** 167–73
[18] Ohhata Y, Shinoki F and Yoshida S 1979 *Thin Solid Films* **59** 255–61
[19] Wu W F and Chiou B S 1993 *Appl. Surf. Sci.* **68** 497–504

[20] Mergel D, Stass W, Ehl G and Barthel D 2000, *J. Appl. Phys.* **88** 2437–42
[21] Rauf I A and Yuan J 1995 *Mater. Lett.* **25** 217–22
[22] Dietrich A, Schmalzbauer K, Hoffmann H and Szczyrbowski J 1984 *Thin Solid Films* **122** 19–29
[23] Odaka H, Shigesato Y, Murakami T and Iwata S 2001 *Japan. J. Appl. Phys.* **40** 3231–5
[24] Mergel D, Buschendorf D, Eggert S, Grammes R and Samset B 2000 *Thin Solid Films* **371** 218–24
[25] Mergel D 2001 *Thin Solid Films* **397** 216–22